Q. J. R. Meteorol. Soc. (2000), **126**, pp. 725–748

Variational cloud-clearing with TOVS data

By J. JOINER* and L. ROKKE
NASA/Goddard Space Flight Center, USA

(Received 7 August 1998; revised 5 May 1999)

SUMMARY

A number of studies have shown that the use of passive microwave and infrared satellite observations in data assimilation systems can increase forecast skill. Considerable effort has been expended over the past two decades, particularly with the TIROS Operational Vertical Sounder (TOVS), to achieve this result. The positive impact on forecast skill is a result of more rigorous treatment of quality control, improvements in systematic error correction schemes, and advances in data assimilation systems. Yet, there still remains potential for improving the use of satellite data, particularly cloud-contaminated observations, in data assimilation. Here, we use a one-dimensional variational framework (1DVAR) as a first step towards improving the treatment of cloudy data by cloud-clearing. Cloud-clearing is a procedure that removes cloud radiative effects through comparison of partly cloudy adjacent pixels. The 1DVAR approach simultaneously extracts cloud-clearing parameters and information about the atmospheric and surface state from microwave and infrared observations. The variational framework ensures that the state estimate is consistent with all available measurements. The 1DVAR cloud-clearing approach can also be extended to three or four dimensions (3DVAR, 4DVAR). Our TOVS cloud-clearing implementation allows for complex cloud structures, including multiple cloud layers with wavelength-dependent radiative properties. We present preliminary results of our 1DVAR cloud-clearing implementation with TOVS. The results suggest that there is useful information in the cloud-cleared data.

KEYWORDS: Variational assimilation Cloud clearing TOVS

1. INTRODUCTION

Data assimilation systems (DAS) have used information contained in the spectral radiance measurements from the TIROS Operational Vertical Sounder (TOVS) extensively for numerical weather prediction (NWP) and Earth Systems studies (e.g. Eyre *et al.* 1993; Derber and Wu 1998; Andersson *et al.* 1998). TOVS radiance information has been assimilated through variational approaches in one dimension (1DVAR) (e.g. Eyre *et al.* 1993) and three- and four-dimensions (3DVAR, 4DVAR) (e.g. Andersson *et al.* 1994, 1998; Derber and Wu 1998). These implementations have relied primarily on cloud-cleared radiances provided by the NOAA National Environmental Satellite Data and Information Service (NESDIS). Cloud-clearing refers to the procedure of removing the effect of cloud from infrared measurements. Cloud-cleared radiances (also referred to as clear-column radiances) are therefore radiances emitted from the cloud-free portion of a satellite footprint.

The assimilation of cloud-cleared observations should not degrade forecast skill. However, NWP experiments have shown that forecast skill increases when some or all of the NESDIS cloud-cleared observations are withheld from the DAS (R. Saunders, private communication, 1997; J. Derber, private communication, 1997). Biases and other errors in the cloud-clearing procedure may be contributing to this effect. Therefore, to make better use of cloud-contaminated observations we must make improvements in cloud-clearing techniques, quality control, systematic error correction, etc.

Discarding cloudy observations is not desirable, because it eliminates a significant fraction of infrared data. Wylie *et al.* (1994) found that only 23% of pixels from the TOVS High-resolution Radiation Sounder 2 (HIRS2) are cloud free. Withholding cloud-cleared observations is especially unappealing for analyses that are used for Earth Systems studies. In particular, information about middle and upper tropospheric humidity derived from infrared observations in cloudy areas will be lost.

* Corresponding author: Data Assimilation Office, Code 910.3, NASA/Goddard Space Flight Center, Greenbelt, Maryland 20771, USA. e-mail: joiner@hera.gsfc.nasa.gov

In this paper, we describe how a variational approach can be used to simultaneously cloud-clear infrared observations and retrieve information about the atmospheric and surface state. This approach unifies existing cloud-clearing techniques with the variational framework by introducing cloud-clearing parameters into the state vector to be estimated. The approach allows for a solution that is consistent with all available spectral measurements. The variational framework is also capable of fully accounting for the non-linear effect of cloud on infrared brightness temperatures. Our cloud-clearing approach is implemented in one dimension (1DVAR). The 1DVAR information may be assimilated or may serve as a pre-processing step for 3DVAR or 4DVAR. The variational cloud-clearing technique can also be extended to three and four dimensions. Here, we focus only on the off-line 1DVAR analysis (i.e. no data assimilation). The ultimate usefulness of the method can only be assessed in data assimilation mode which is beyond the scope of the present study.

Our cloud-clearing implementation with TOVS can deal with the complex radiative and physical properties of clouds. For example, our approach can handle multiple levels of clouds with different relative cloud fractions in adjacent fields-of-view. Previous cloud-clearing implementations with TOVS have been more limited in terms of dealing with complex cloud structures. Our approach also makes no assumptions or simplifications regarding the spectral radiative properties of clouds.

The outline of the paper is as follows: Section 2 reviews the TOVS instrument package, clear-sky radiative transfer, cloud-clearing, and the variational framework. We describe the details of the 1DVAR implementation with TOVS data in section 3. Preliminary results are presented in section 4. Future work is discussed in the last section.

2. Background

(*a*) *The TOVS instrument package*

TOVS consists of three separate sounding instruments: (1) The High-resolution Infrared Radiation Sounder 2 (HIRS2) (2) The Microwave Sounding Unit (MSU) (3) The Stratospheric Sounding Unit (SSU) (Smith *et al.* 1979). TOVS has flown on the TIROS-N satellite and on National Oceanic and Atmospheric Administration (NOAA) operational polar-orbiting environmental satellites (POES) 6–12 and 14. NOAA 10 and 12 did not have an SSU instrument. An Advanced TOVS (ATOVS) with a HIRS instrument (HIRS3) and the Advanced Microwave Sounding Unit (AMSU) has been launched on NOAA 15.

The TOVS instruments measure the radiance from Earth passively in spectral elements or channels. The measured radiance includes thermal emission in the microwave and infrared channels and reflected solar radiation in the visible and shorter wavelength infrared channels. Radiance is commonly expressed in terms of equivalent blackbody temperature (brightness temperature), because brightness temperature is a more linear function of the atmospheric temperature and other parameters than radiance.

HIRS2 has 19 infrared channels with centre frequencies ranging from approximately 670 to 2660 cm^{-1} and one visible channel. MSU has four channels centred near the 57 GHz oxygen cluster. SSU employs the pressure modulation technique to measure stratospheric emission in three channels of the 15 μm CO_2 band.

All three TOVS instruments scan cross track. The maximum instrument scan angles (from nadir) are approximately 51° (HIRS2), 57° (MSU), and 45° (SSU). The footprint sizes of HIRS2, MSU, and SSU are approximately 17.4, 124, and 147 km at nadir, respectively.

(*b*) *Clear-sky radiative transfer*

A radiative transfer model provides the means to relate state variables, such as temperature and humidity, to radiance observations. The calculation of radiance and its Jacobian is a computationally burdensome portion of any physically-based state estimation with TOVS and similar sounders. It is not feasible to process TOVS data operationally with monochromatic calculations (also referred to as line-by-line models). Therefore, as in most operational settings, we use a fast transmittance model (FTM) (McMillin and Fleming 1976).

In this study we use a FTM referred to as the Goddard Laboratory for Atmosphere TOVS (GLATOVS) radiative transfer algorithm (Susskind *et al.* 1983; Sienkiewicz 1996). GLATOVS is similar to the RTTOV FTM (Eyre 1991; Saunders *et al.* 1999) that has been used extensively in NWP (e.g. Eyre *et al.* 1993; Derber and Wu 1998). GLATOVS includes treatment of the reflected solar and downwelling radiation. The absorption is computed for gases assumed to be in a fixed distribution, such as CO_2, N_2O, and N_2. The absorption is also computed for H_2O and O_3 whose vertical distributions must be specified.

(*c*) *Cloud-clearing*

Cloud-clearing refers to the process of estimating what the radiance would have been in the absence of cloud. Eyre and Watts (1987) provide a detailed review of several cloud-clearing methods. Here we use an extension of the adjacent field-of-view (FOV) approach developed by Smith (1968) and Chahine (1974, 1977) which we will now review.

(i) *Cloudy radiances.* The satellite-observed radiance in a partially cloudy pixel consists of the radiance coming from the cloud-free portion of the scene and radiance from areas covered by different kinds of clouds, weighted by their corresponding fractional areas. An example is illustrated in Fig. 1. The observed radiance, $\overline{\mathbf{R}}_i^k$, in channel i and in field-of-view k in a scene with J different cloud types can be expressed as

$$\overline{\mathbf{R}}_i^k = \left(1 - \sum_{j=1}^{J} \alpha_j^k\right) \mathbf{R}_i^{\mathrm{CLR}} + \sum_{j=1}^{J} \alpha_j^k \mathbf{R}_{i,j}^{\mathrm{CLD}} \tag{1}$$

where α_j^k is the cloud type j fraction, $\mathbf{R}_i^{\mathrm{CLR}}$ is the clear-column radiance, and $\mathbf{R}_{i,j}^{\mathrm{CLD}}$ is the radiance coming from the α_j^k fraction of the scene corresponding to cloud type j. $\mathbf{R}_i^{\mathrm{CLR}}$ can be modelled with an FTM. In general, $\mathbf{R}_{i,j}^{\mathrm{CLD}}$ may have complex wavelength-dependent spectral properties.

In (1), a cloud type may refer to either a single cloud layer or a multiple-layer cloud formation. A cloud layer refers to a structure that produces a particular radiance signature. For example a cloud layer may be cirrus cloud in some altitude range with emissivity less than 1. A cloud formation refers to a linear combination of cloud layers. For example, a cloud formation could be a structure with two cloud layers, where one layer covers half the area of the other.

(ii) *Adjacent field-of-view approach.* In this cloud-clearing approach, two or more adjacent HIRS fields-of-view (FOVs) are used, where each FOV produces a different realization of (1). The FOVs are assumed to be homogeneous except for the amount of cloud cover, i.e. it is assumed that $\mathbf{R}_i^{\mathrm{CLR}}$ and $\mathbf{R}_{i,j}^{\mathrm{CLD}}$ in each FOV are equal but that the

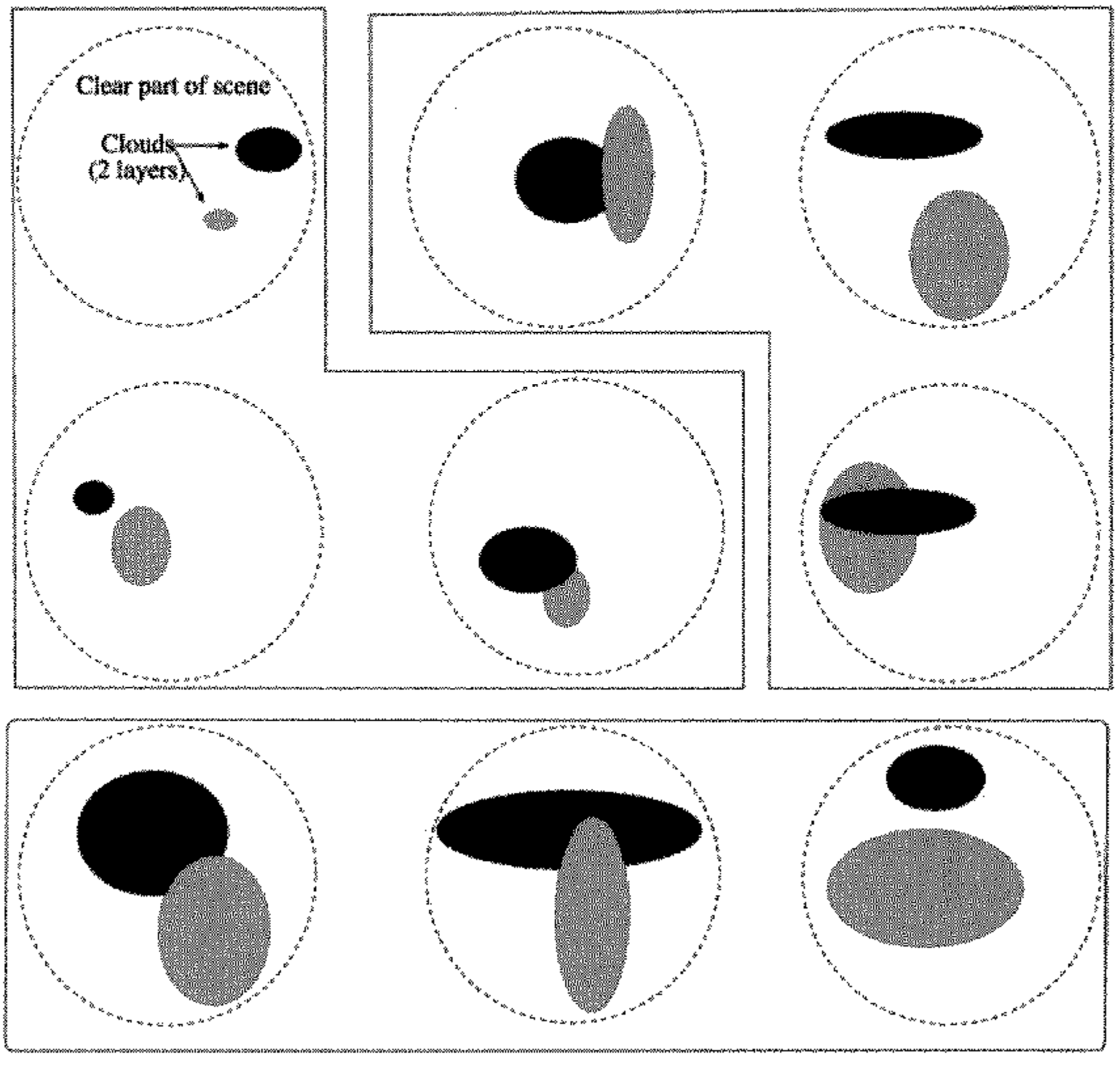

Figure 1. Sample array of nine HIRS pixels showing how the pixels are sorted and grouped to form three fields-of-view for cloud clearing. The radiance emitted by each pixel has a component coming from a clear part of the scene and components coming from different cloud layers.

α_j^k (for each j) are not. This assumes that the radiative spatial variability of cloud cover is much larger than that of the atmospheric and surface parameters. It is also assumed that the α_j^k for each cloud formation are distinct in at least two fields-of-view. Therefore, each cloud formation may contain a complex distribution of heights (which may affect radiation in a complex manner). However, we assume that the radiation from each cloud formation is the same in all fields-of-view (i.e. that each cloud formation is the same in every FOV). It is assumed that only the amount of each cloud formation varies between the different FOVs.

With these assumptions, the reconstructed clear-column radiance for channel i, $\widehat{\mathbf{R}}_i^{\mathrm{CLR}}$, can be written as a linear combination of the measured radiances in $K + 1$ fields-of-view, $\overline{\mathbf{R}}_{i,1} \ldots \overline{\mathbf{R}}_{i,K+1}$, i.e.

$$\widehat{\mathbf{R}}_i^{\mathrm{CLR}} = \overline{\mathbf{R}}_{i,1} + \eta_1(\overline{\mathbf{R}}_{i,1} - \overline{\mathbf{R}}_{i,2}) + \eta_2(\overline{\mathbf{R}}_{i,1} - \overline{\mathbf{R}}_{i,3}) + \cdots + \eta_K(\overline{\mathbf{R}}_{i,1} - \overline{\mathbf{R}}_{i,K+1}) \quad (2)$$

(Chahine 1977), where $\eta_1 \ldots \eta_K$ are channel-independent constants because they depend only on the α's. In general, $K + 1$ fields-of-view are required to obtain information about K cloud formations.

There are a few potential problems with this approach that should be considered. For example, surface heterogeneity may produce surface clearing rather than the desired cloud clearing. However, this is not a severe problem because surface clearing in effect will clear one surface type from the others. Therefore, it still produces clear radiances,

but with more noise than if the scenes were declared clear. The usefulness of cloud-cleared data over land will have to be evaluated in data assimilation experiments. Currently, several NWP centres do not assimilate information from surface sensitive channels over land.

The cloud-cleared data is also representative only of the clear portion of the footprint, not necessarily of the entire footprint. This could create biases, especially in humidity. However, this bias is likely to be much smaller than the bias in the background humidity field.

(iii) *Previous implementations.* The general approach that has been used previously to solve for $\eta_1 \ldots \eta_K$ involves the following steps (e.g. Chahine 1977): (1) Estimate the clear-column radiance for a subset of infrared channels. Microwave channels, assumed to be unaffected by cloud, are often used in this step (e.g. McMillin and Dean 1982; Susskind *et al.* 1984). The effect of non-precipitating cloud on MSU channels is small and therefore MSU observations can be used to adjust the temperature profile or predict HIRS clear-column brightness temperatures. (2) Invert Eq. (2) by least-squares or some other method to obtain an estimate of $\eta_1 \ldots \eta_K$. (3) Reconstruct the clear-column radiances for all infrared channels using Eq. (2). (4) Retrieve additional information about the atmospheric and surface state using the reconstructed clear-column radiances and other cloud-free observations. (5) Repeat steps (1)–(4) using the improved state estimate. Step (5) is optimal and has been used with TOVS data by Susskind *et al.* (1984).

Cloud-clearing, based on this general approach, has been applied with several real and proposed instruments with different numbers of fields-of-view (i.e. different degrees of freedom for cloud formations). Cloud-clearing has been applied to HIRS2/MSU observations with $K = 1$, i.e. two FOVs allowing for one cloud formation (e.g. Susskind *et al.* 1984; McMillin and Dean 1982). Simulations have been performed with two cloud formations and three FOVs for the proposed AMTS instrument in combination with MSU (Susskind and Reuter 1985). Chahine *et al.* (1977) applied the method with four FOVs using an experimental airborne 18 channel grating spectrometer.

(*d*) *Variational framework*

Many data assimilation systems use a variational framework to estimate the atmospheric and surface state from a set of observations and a background estimate. In NWP, the background is typically a short-term forecast from a prediction model. Here we will use the variational framework to simultaneously estimate the cloud-clearing parameters (η's) from the previous section and the atmospheric and surface parameters affecting satellite-observed radiances.

(i) *Variational formulation.* In the variational approach (e.g. Lorenc 1986; Talagrand 1988), one minimizes a penalty or likelihood function J with respect to the atmospheric state vector $\mathbf{x}$ or increment from the background $\delta\mathbf{x}$, i.e.

$$J(\delta\mathbf{x}) = \tfrac{1}{2}\delta\mathbf{x}^{\mathrm{T}}\mathbf{B}^{-1}\delta\mathbf{x} + \tfrac{1}{2}(\mathbf{H}\delta\mathbf{x} - \mathbf{d})^{\mathrm{T}}\mathbf{R}^{-1}(\mathbf{H}\delta\mathbf{x} - \mathbf{d}), \tag{3}$$

where $\mathbf{B}$ is the background error covariance, $\mathbf{H}$ is the linearized observation operator, $\mathbf{d}$ is the innovation vector, and $\mathbf{R}$ is the observation error covariance. The innovation vector is defined as

$$\mathbf{d} = \mathbf{y}^{\mathrm{o}} - \mathbf{H}\mathbf{x}^{\mathrm{b}}, \tag{4}$$

where $\mathbf{y}^o$ is the observation vector and $\mathbf{x}^b$ is the background vector. The analysis $\mathbf{x}^a$ after minimization is given as

$$\mathbf{x}^a = \mathbf{x}^b + \delta\mathbf{x}^a. \tag{5}$$

The minimum of $J(\delta\mathbf{x})$ is the mode of the conditional probability density function $p(\mathbf{x}|\mathbf{x}^b \cup \mathbf{y}^o)$ (Jazwinski 1970). This assumes that covariances are specified correctly and that the forecast and observation errors are unbiased, normally distributed, and uncorrelated with each other.

(ii) *Quasi-Newton iterative scheme.* In our application the observation operator, $\mathrm{h}(\mathbf{x})$, includes the non-linear fast radiative transfer model. The minimum of $J(\delta\mathbf{x})$ for a nonlinear observation operator can be obtained by a quasi-Newton iteration of the form

$$\begin{aligned}\mathbf{x}_{i+1} &= \mathbf{x}^b + (\mathbf{H}_i^T(\mathbf{R})^{-1}\mathbf{H}_i + (\mathbf{B})^{-1})^{-1}\mathbf{H}_i^T(\mathbf{R})^{-1}[\mathbf{y}^o(\mathbf{x}_i) - \mathrm{h}(\mathbf{x}_i) + \mathbf{H}_i(\mathbf{x}_i - \mathbf{x}^b)] \\ &= \mathbf{x}^b + \mathbf{B}\mathbf{H}_i^T(\mathbf{H}_i\mathbf{B}\mathbf{H}_i^T + \mathbf{R})^{-1}[\mathbf{y}^o(\mathbf{x}_i) - \mathrm{h}(\mathbf{x}_i) + \mathbf{H}_i(\mathbf{x}_i - \mathbf{x}^b)]\end{aligned} \tag{6}$$

(e.g. Rodgers 1976) where

$$\mathbf{H}_i = \left.\frac{\partial \mathrm{h}(\mathbf{x})}{\partial \mathbf{x}}\right|_{\mathbf{x}=\mathbf{x}_i}. \tag{7}$$

The analysis vector, $\mathbf{x}^a$, that minimizes $J(\delta\mathbf{x})$ is

$$\mathbf{x}^a = \lim_{i\to\infty} \mathbf{x}_i. \tag{8}$$

The analysis error covariance, $\mathbf{P}^a$, at convergence (dropping the iteration subscript) is

$$\mathbf{P}^a = (\mathbf{H}^T(\mathbf{R})^{-1}\mathbf{H} + (\mathbf{B})^{-1})^{-1}. \tag{9}$$

The formulation of (6) is more general than usually appears in the literature. Here, instead of assuming the observations to be fixed, we allow the observations to be a function of the current state estimate.

We use the first form of (6) in our implementation. This is desirable because the error covariance estimate given by (9) requires no additional computation. We also found that preconditioning was necessary to solve (6) by the second formulation while it was not necessary with the first formulation. Although slightly more expensive than the second form of (6) for our state and observations vector, the first form will be much less computationally expensive for future high-spectral-resolution sounders with orders of magnitude more spectral elements than TOVS.

(iii) *Previous implementations.* Eyre *et al.* (1993) used a 1DVAR approach with TOVS clear and cloud-cleared brightness temperatures to estimate a state vector consisting of mean-layer temperatures and humidities, the surface skin and surface air temperature, and surface pressure. Eyre (1989a,b) applied 1DVAR to cloudy TOVS radiances with effective cloud-top pressure and cloud amount added to the previously described state vector. In that work, Eyre (1989a,b) assumed a single cloud layer with wavelength-independent cloud emissivity and negligible reflected solar radiation. Here, we eliminate the need to parameterize cloud radiative properties in the state vector. This is accomplished by using the adjacent FOV cloud-clearing approach described above within the 1DVAR framework.

3. 1DVAR CLOUD-CLEARING WITH TOVS

In our 1DVAR implementation, unprocessed TOVS observations known as level 1b data are used. These data consist of uncalibrated observations, calibration coefficients, and appended Earth location information provided by NESDIS (Kidwell 1997).

The TOVS 1DVAR implementation involves several steps including pre-processing, quality control, and systematic error correction. Our approach brings together many aspects of the cloud-clearing work of e.g. Susskind *et al.* (1984) and McMillin and Dean (1982) and of the variational approaches used by e.g. Eyre *et al.* (1993). For completeness, we describe each step in detail below.

(*a*) *Pre-processing*

The first pre-processing step is to produce collocated HIRS, MSU, and SSU radiances from the uncalibrated observations. We apply the calibration constants provided in the level 1b data to the raw observations to derive radiances or brightness temperatures for HIRS, MSU, and SSU. The calibration constants are monitored to detect instrument anomalies or failure.

The next step is to organize individual HIRS pixels into a specified number of adjacent fields-of-view. First, we subset HIRS pixels into a series of rectangles. Figure 1 shows the example used in this study where the rectangle (square) is always a 3×3 array of HIRS pixels. We then attempt to sort and group the pixels within the array according to the amount of cloudiness. In this work, we always sort the nine spot rectangle into three FOVs, where each FOV is an average of three pixels. In Fig. 1, we show an example of grouping the three spots with the smallest amount of cloud cover, the three spots with the largest amount cloud cover, and the three spots in between. To accomplish this sorting, we use the brightness temperature in HIRS 8. HIRS 8 is centred in the 11 μm window region, where the earth's atmosphere is relatively transparent and solar radiation is negligible. Because clouds in general emit radiation at cooler temperatures than the surface, the brightness temperature in HIRS 8 will decrease with increasing cloud cover. The approach is still valid even if the cloud is warmer than the underlying surface and the ordering of the FOVs is from clearest to cloudiest.

Once sorted and grouped, pixels are averaged to produce radiances in the desired number of fields-of-view. The averaging process creates in effect a super-observation with a larger footprint and perhaps a slightly different cloud fraction. Averaging FOVs reduces the impact of random instrumental error and enhances the radiance contrast between the fields-of-view. This is desirable, because it reduces the noise amplification effect produced by cloud-clearing. Here, we average the radiances in each of the three groupings for each channel as shown in Fig. 1 to produce radiances in three fields-of-view.

The next step is to collocate HIRS, MSU, and SSU observations. This is accomplished by selecting the MSU or SSU pixel closest to the centroid of a HIRS pixel array. The collocation is acceptable if the chordal distance between the HIRS and MSU/SSU observation is less than 1°. The appropriate satellite zenith angle for each instrument is used in radiative transfer calculations (i.e. there will be a different angle for HIRS, MSU, and SSU).

We do not interpolate or extrapolate MSU or SSU observations to HIRS fields-of-view. NESDIS maps both MSU and SSU data to HIRS FOVs. This is a particular problem for the SSU instrument. SSU has a more limited scan range than both the MSU and HIRS. NESDIS requires SSU radiances for its temperature retrievals and therefore extrapolates from the last SSU radiance to the end of the HIRS scan track. The SSU

instrument did not fly on all POES satellites. In these cases, NESDIS uses a climatological mapping to provide SSU radiances where none are available. Furthermore, NESDIS also adjusts TOVS radiances to those that would have been observed at nadir view. Additional adjustments have been made to the radiances of some channels to estimate those that would have been observed with unit surface emissivity. These adjustments, made to the actual observations, and the creation of climatological SSU observations can create significant systematic errors (A. Reale, private communication, 1997; Wu and McAvaney 1998; McNally *et al.* 2000).

(*b*) *1DVAR implementation*

(i) *State vector.* The state vector for each sounding is defined at the centroid of the HIRS pixel array. Our state vector consists of 17 layer-mean temperatures from the surface to 0.4 mb, 13 layer-mean values of the natural log of the specific humidity from the surface to 10 mb, 13 layer amounts of the natural log of column ozone from the surface to 0.4 mb, surface skin temperature (T_s), microwave emissivity (ϵ_{mw}), infrared bi-directional reflectance (ρ) in the presence of sunlight, and two cloud-clearing parameters (η_1 and η_2) in cases determined to be cloudy. It is straight-forward to modify the state vector to accommodate additional variables such as a more complex microwave emissivity model or an increase in the number of cloud-clearing parameters or layers.

The augmentation of the state vector by the addition of K cloud-clearing parameters should decrease the information content of the observations with respect to the other state variables. This effect, however, is offset in part by using observations in $K + 1$ fields-of-view. The information content of the observations with respect to atmospheric and surface parameters does decrease as the radiance contrast between the FOVs decreases. This decrease in information content is realized by properly accounting for the increase in brightness temperature error introduced by the cloud-clearing process. Details are given in the next section.

(ii) *Observation vector and covariance.* Our observation vector consists of all available MSU and SSU brightness temperature observations and clear-column brightness temperatures for selected HIRS channels (1–15, 18–19). HIRS channels 16–17 are excluded, because of significant biases that could not be removed. The clear-column HIRS brightness temperature depends on the cloud-clearing parameters. Therefore, the observation vector depends on the current state estimate.

Cloud-clearing should only be applied to channels affected by cloud. This is because cloud-clearing is an extrapolation process that amplifies measurement error. We attempt to determine whether or not certain channels (HIRS 1–4) are cloud-free under partially cloudy conditions. All other HIRS channels are assumed to be cloud-contaminated in a cloudy scene. HIRS 1–4 have weighting functions that peak at approximately 400 mb and above. A channel is declared cloud-free if the absolute value of the radiance difference between the warmest and coldest FOV is less than $\sqrt{2}$ times the detector noise. This value was chosen empirically so that if the FOV variance is greater than the approximate expected value in a clear scene, the channel is assumed to be cloud-contaminated. We check HIRS channels 1–4 for cloud contamination in order of decreasing peak pressure of the weighting function. If a channel is determined to be cloud-free, then all channels with peak weighting function pressures above are also assumed cloud-free. For cloud-free channels, $\eta_1 \ldots \eta_K$ are set equal to $-1/(K + 1)$ in (2). This is equivalent to averaging radiances in the $K + 1$ fields-of-view.

The observation error covariance is the sum of the measurement error covariance and the observation operator error covariance (e.g. Eyre 1993). We will consider the

measurement error to be the sum of two components: (1) detector noise (2) scene noise resulting from inhomogeneity in the fields-of-view. For MSU and SSU, the scene noise is zero because there is only one pixel per sounding. We estimated the observation operator error using collocated radiosonde data.

Both the measurement and observation operator error covariances are assumed to be diagonal (i.e. no inter-channel correlation). This is probably a valid assumption for the measurement error but not necessarily for the observation operator error. In addition, small amounts of cloud in scenes determined to be clear or residual uncleared cloud will lead to channel correlated errors. The former case could also occur when assimilating only clear radiances. To check the sensitivity to assumed channel correlated errors, experiments were performed with a non-diagonal observation operator covariance estimated with radiance departures from collocated radiosondes. No significant improvement was achieved in these experiments.

The amplification of the measurement error by cloud-clearing must be considered for HIRS channels. For these channels, the observation is the brightness temperature corresponding to estimated clear-column radiance given by (2). The measurement error variance that applies to the estimated clear-column radiance should be multiplied by an amplification factor. From (2), the derived amplification factor A is given by

$$A = \left(1 + \sum_{k=1}^{K} \eta_k\right)^2 + \sum_{k=1}^{K} \eta_k^2. \tag{10}$$

From (10), it is evident that the larger the values of the η's, the larger the noise amplification effect will be. It can be shown that $\eta_1 \to \infty$ as $\alpha_1^1 \to \alpha_2^1$. Therefore, as the contrast between the two FOVs goes to zero, the cloud-clearing problem becomes ill-posed. In (iv), we outline the criteria used to determine in which situations cloud-clearing should be applied.

We model the total observation error variance for HIRS cloud-cleared channel i, denoted σ_1^2, according to

$$\sigma_i^2 = \left[\sqrt{([\sigma_{d_i}]^2 + [\sigma_{\mathrm{FOV}_i}(\partial B_i/\partial T)]^2)A}\left(\frac{\partial B_i}{\partial T}\right)^{-1}\Bigg|_{T=T_{b_i}^{\mathrm{clr}}}\right]^2 + [\sigma_{c_i}]^2, \tag{11}$$

where σ_d is the detector noise standard deviation given in radiance units, σ_{FOV} is the scene noise given in Kelvins, B is the Planck function evaluated at the clear-column brightness temperature T_b^{clr}, and σ_c is the observation operator error standard deviation given in Kelvins. In (11), only the measurement error (in radiance units) is amplified by the factor A. The amplified measurement error variance is then converted to brightness temperature units and added to the observation operator error variance. Table 1 lists the standard deviations for all components of the observational errors used in our 1DVAR. Typical values of σ_d converted to equivalent temperature are given. Also provided are sample values for a clear scene and a scene with noise amplification ($\sqrt{A} = 2$). The detector noise is based on instrument specifications. The scene noise was empirically specified. The observation operator errors were estimated using collocated radiosonde data.

In the cloudy case, the amplification of scene and detector noise dominates the overall error. We have been rather conservative in using the instrument specified noise rather than measured values which are typically lower. We have also probably overestimated the scene noise for channels that are not sensitive to surface effects. In the future, these

TABLE 1. COMPONENTS OF THE OBSERVATIONAL ERROR USED IN 1DVAR. THE THIRD, SIXTH, AND SEVENTH COLUMNS REPRESENT TYPICAL (TYP) VALUES OF NOISE FOR A CLEAR (CLR) AND CLOUDY (CLD) SCENE.

channel	σ_d mw/m^2-ster-cm^{-1}	σ_d (typ) (K)	σ_{FOV} (K)	σ_c (K)	σ_{clr} (typ) (K)	σ_{cld}, $\sqrt{A}=2$ (K)
HIRS 1	3.00	2.52	0.5	1.0	1.79	5.23
HIRS 2	0.67	0.62	0.5	1.0	1.10	1.89
HIRS 3	0.50	0.48	0.5	0.7	0.81	1.55
HIRS 4	0.31	0.30	0.5	0.3	0.45	1.21
HIRS 5	0.21	0.19	0.5	0.5	0.59	1.18
HIRS 6	0.24	0.20	0.5	0.7	0.77	1.28
HIRS 7	0.20	0.15	0.5	0.8	0.86	1.31
HIRS 8	0.10	0.07	0.5	0.3	0.42	1.05
HIRS 9	0.10	0.11	0.5	0.5	0.58	1.14
HIRS 10	0.16	0.10	0.5	0.3	0.42	1.06
HIRS 11	0.20	0.51	0.5	1.2	1.27	1.86
HIRS 12	0.20	1.21	0.5	1.5	1.68	3.03
HIRS 13	0.006	0.13	0.5	0.4	0.50	1.11
HIRS 14	0.003	0.12	0.5	0.3	0.42	1.07
HIRS 15	0.004	0.17	0.5	0.3	0.43	1.10
HIRS 18	0.002	0.10	0.5	0.4	0.50	1.09
HIRS 19	0.002	0.10	0.5	0.3	0.42	1.06
MSU 1	N/A	0.35	0.0	0.2	0.40	N/A
MSU 2	N/A	0.33	0.0	0.4	0.52	N/A
MSU 3	N/A	0.22	0.0	0.5	0.73	N/A
MSU 4	N/A	0.28	0.0	0.8	1.04	N/A
SSU 1	0.30	0.24	0.0	0.4	0.47	N/A
SSU 2	0.40	0.29	0.0	0.4	0.50	N/A
SSU 3	1.00	0.73	0.0	0.4	0.83	N/A

TABLE 2. 1DVAR TEMPERATURE AND HUMIDITY BACKGROUND ERROR STANDARD DEVIATIONS, σ_t AND σ_q RESPECTIVELY (UNIT OF HUMIDITY IS NATURAL LOG OF SPECIFIC HUMIDITY)

p (mb)	1000	850	750	500	400	300	250	200	150	100	70	50	30	10	5	2	1	0.4
σ_t (K)	0.90	0.85	0.73	0.66	0.68	0.70	0.85	0.85	0.65	0.60	0.64	0.7	0.7	0.9	1.1	1.3	1.5	1.8
σ_q	0.10	0.12	0.15	0.20	0.25	0.30	0.45	0.60	0.70	0.70	0.70	0.70	0.70	0.70				

values may be changed which will give more weight to the measurements in cloudy situations.

For cloud-free channels, setting $\eta_1 \ldots \eta_K = -1/(K+1)$ in (10) results in $A = [1/(K+1)]$. Because this averages radiances in the $K+1$ fields-of-view, it reduces the radiance measurement error variance (but not the observation operator error variance) by a factor of $K+1$.

(iii) *Background vector and covariance.* A six-hour forecast from the GEOS model serves as the background for atmospheric temperature (derived hydrostatically from geopotential height), humidity, and surface (skin) temperature. The sea surface temperatures are from the monthly analysis of Reynolds (1988). We use a 70-level version of the GEOS model. The model extends from the surface to 0.01 mb. The 70-level temperature and humidity profiles specified on σ levels are interpolated to the analysis levels given in Table 2. The model spatial resolution is 2° latitude × 2.5° longitude. Takacs *et al.* (1994) describe the GEOS model in detail.

A stationary (state-independent) covariance model is used for the background atmospheric temperature and humidity on the analysis levels. The standard deviations are listed in Table 2. The variances and covariances are similar to those used by Eyre *et al.* (1993). We assume no correlation between temperature and humidity errors.

Layer-mean values are generated by averaging the level data linearly in $\ln(p)$. The background error variances have been adjusted empirically based on comparisons with collocated radiosondes.

The variance of the background T_s is set to $(8\text{K})^2$ over land and sea ice and $(2\text{K})^2$ over ocean. Smith *et al.* (1996) have shown daily variability in the ocean surface skin temperature of this magnitude. We assume no correlation between the T_s and other state variable errors. The first guess ϵ_{mw} is set to 0.9 over land and to 0.55 over ocean and ρ to 0.05 (daytime only). Both ϵ_{mw} and ρ are well-determined by the observations. Therefore, we set their background variances a large value $(10^8)^2$. This gives essentially no weight to the initial guess. The infrared surface emissivity is assumed to be known. Over sea, the emissivity is set to be 0.98 for HIRS 1–12 and 0.95 for HIRS 13–19. We plan to add a scan-angle dependent model for ocean emissivity in the future. We use emissivities of 0.95 for HIRS 1–9, 0.90 for HIRS 10–12, and 0.85 for HIRS 13–19 over land including snow (Susskind *et al.* 1983).

To obtain a first guess for the cloud-clearing parameters $(\eta_1^0 \ldots \eta_K^0)$, we use (2) for a given set of channels, i.e.

$$\begin{pmatrix} \tilde{R}_1^{\mathrm{CLR}} - \overline{R}_{1,1} \\ \tilde{R}_2^{\mathrm{CLR}} - \overline{R}_{2,1} \\ \vdots \\ \tilde{R}_I^{\mathrm{CLR}} - \overline{R}_{I,1} \end{pmatrix} = \begin{pmatrix} \overline{R}_{1,1} - \overline{R}_{1,2} & \overline{R}_{1,1} - \overline{R}_{1,3} & \ldots & \overline{R}_{1,1} - \overline{R}_{1,K+1} \\ \overline{R}_{2,1} - \overline{R}_{2,2} & \overline{R}_{2,1} - \overline{R}_{2,3} & \ldots & \overline{R}_{2,1} - \overline{R}_{2,K+1} \\ \vdots & \vdots & \ddots & \vdots \\ \overline{R}_{I,1} - \overline{R}_{I,2} & \overline{R}_{I,1} - \overline{R}_{I,3} & \ldots & \overline{R}_{I,1} - \overline{R}_{I,K+1} \end{pmatrix} \begin{pmatrix} \eta_1^0 \\ \eta_2^0 \\ \vdots \\ \eta_K^0 \end{pmatrix} \tag{12}$$

where $\tilde{R}_i^{\mathrm{CLR}}$ are the channel i radiances computed using the background atmospheric and surface state. This set of equations can be solved by least-squares using a diagonal observation error covariance with elements $(\sigma^{\mathrm{o}})^2$ given by

$$(\sigma_{i,i}^{\mathrm{o}})^2 = [\sigma_{\mathrm{d}_i}]^2 + [\sigma_{c_i}(\partial B_i/\partial T)]^2. \tag{13}$$

In this approach, we use HIRS channels previously determined to be affected by cloud. We exclude HIRS 8, 9, 10, 11, 12, 18, and 19, because they may contain significant errors in $\tilde{R}_i^{\mathrm{CLR}}$. These errors result from the effects of relatively large errors in the background surface parameters (especially over land) and/or atmospheric humidity. We set the background variance of $\eta_1 \ldots \eta_K$ equal to $(10^8)^2$, giving no weight to the first guess. Even though no weight is given to the first guess for some of the variables, we found that faster convergence was obtained by using a relatively accurate first guess.

Currently, we use a zonal-mean season-independent climatology as the ozone background. The ozone climatological profiles and covariances were generated from a combination of ozone sonde measurements and retrieved profiles from the Stratospheric Aerosol and Gas Experiment (SAGE) (Chu *et al.* 1989) by S. Cox, private communication (1995). The covariances generated from these data sets are used as the ozone background errors. The column amounts and standard deviations (square root of the diagonal of the error covariance used here) for the six latitude bins are shown in Fig. 2. The lowest values of total-column ozone and variability are found in the tropics. The hemispheric asymmetry results in part from the large ozone loss (ozone hole) at high latitudes in the southern hemisphere spring.

In addition to surface properties, MSU 1 and 2 are also sensitive to cloud liquid water (CLW) and precipitation. Our assumption here is that precipitating scenes will be filtered out in the quality control step and that the errors resulting from CLW effects are negligible. Since we are dealing with partially cloudy scenes, the effect of CLW on

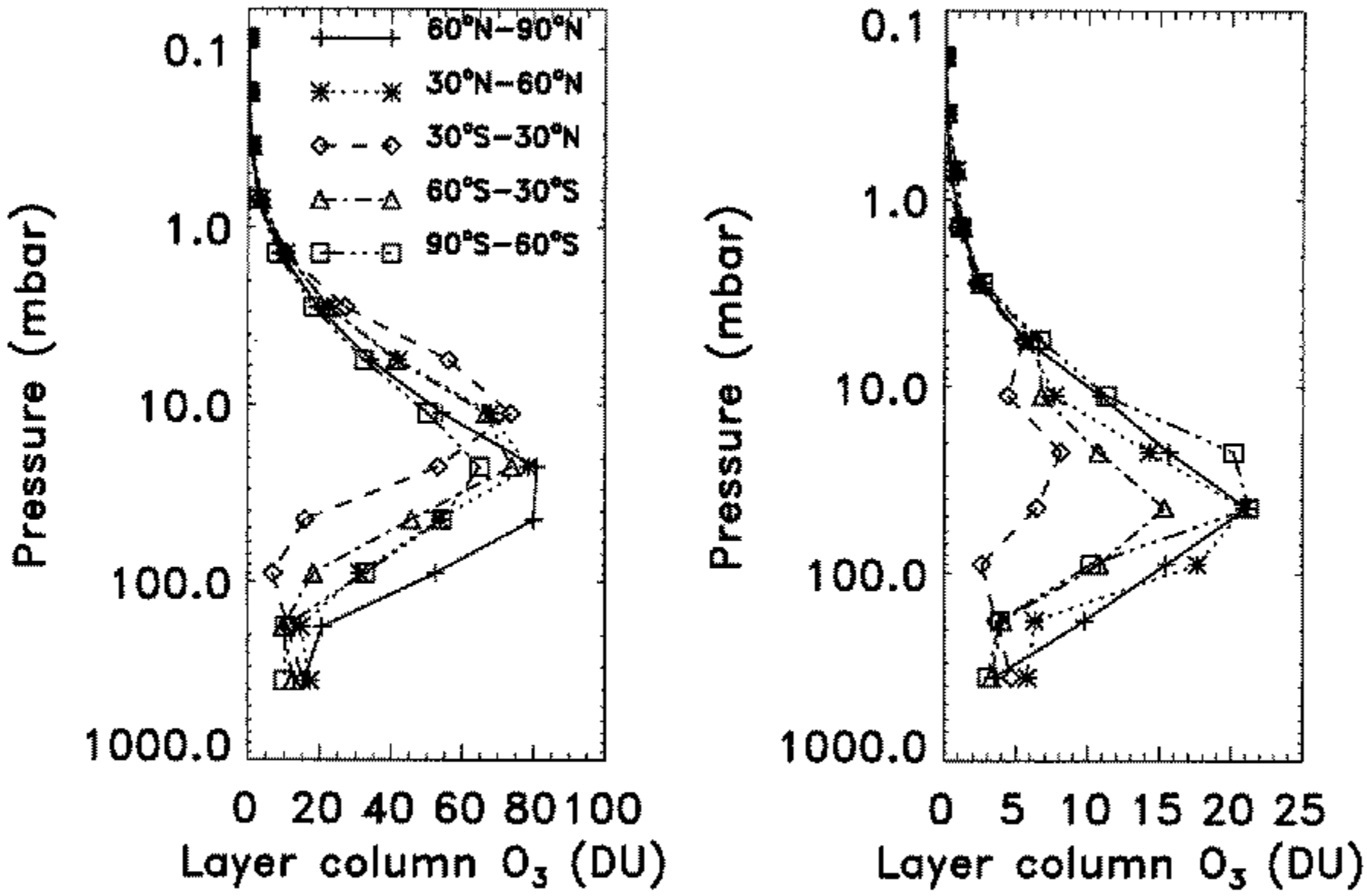

Figure 2. Left: Background layer-integrated ozone for five latitude bins used in 1DVAR. Right: Background standard deviation of layer-integrated ozone.

MSU 2 and 3 should be relatively small. By neglecting CLW in the radiative transfer calculation, this will cause an error in the retrieved microwave emissivity. Because MSU 1 and 2 have slightly different sensitivities to CLW, this will create an error in MSU 2.

(iv) *Observation operator.* The observation operator (and its tangent linear model) consists of two main components: (1) An interpolation operator (2) A fast radiative transfer model. The interpolation operator takes the background fields on the model grid and interpolates them linearly (in space, not in time) to observation locations. The temperature and humidity fields are then interpolated to the fine levels of the fast radiative transfer model. Temperature is interpolated linearly in $\ln(p)$, and humidity is interpolated logarithmically in $\ln(p)$. Ozone is interpolated as log of the cumulative amount (from the top of the atmosphere) in $\ln(p)$.

The fast radiative transfer (RT) model is the GLATOVS package described above. It has 70 levels from 1050 mb to 0.4 mb. Because the background does not always extend to the terrain surface, we have to extrapolate the background for the RT calculations. We assume the surface pressure is fixed and given by values taken from a $0.5° \times 0.5°$ terrain database. This data base gives surface pressures that are more appropriate for the satellite footprint than the lower resolution model surface pressures.

(v) *Cloud detection.* Several tests are performed to determine whether a scene is clear, partly cloudy, or overcast before applying the 1DVAR scheme. We first check the contrast between the warmest and coldest FOV using HIRS 8. If the contrast is less than 2.5 K over land or 2.0 K over ocean, then a series of tests along the lines of McMillin and Dean (1982) is performed to determine if the scene is clear or overcast.

For clear scenes, we exclude $\eta_1 \ldots \eta_K$ from the state vector. In this case, we set $\eta_1 \ldots \eta_K$ equal to $-1/(K+1)$ in (11) and (10). In overcast scenes, we exclude all HIRS channels from the observation vector and exclude $\eta_1 \ldots \eta_K$ from the state vector. In overcast conditions, MSU observations are used only over ocean where we are

confident in our ability to detect rain. To check for rain, ϵ_{mw} is retrieved using MSU 1 with the background state vector. If $\epsilon_{mw} < 0.7$, then the scene is declared to be rain-free and MSU channels are included in the observation vector.

(c) *Quality control*

Quality control is an essential element of any successful DAS and is particularly important for the assimilation of TOVS data (Eyre *et al.* 1993; Derber and Wu 1998; Andersson and Järvinen 1998). In general, when the observations are assimilated, quality control includes an outlier test (the so-called background check) and comparison with neighbouring observations (the so-called buddy check). We would like to eliminate erroneous soundings before they are presented to the DAS. This will more effectively prevent bad observations from being accepted by the DAS. Our objective is to detect and reject cases when our assumptions (e.g. FOV homogeneity, no low cloud present, no rain, etc.) have been violated.

(i) *Convergence check.* To check for convergence within the 1DVAR iterative scheme, at each iteration i, we compute the quantity χ_i^2 given by

$$\chi_i^2 = [\mathbf{y}^o - \mathrm{h}(\mathbf{x}_i)]^T(\mathbf{R})^{-1}[\mathbf{y}^o - \mathrm{h}(\mathbf{x}_i)] + [\mathbf{x}_i - \mathbf{x}_b]^T(\mathbf{B})^{-1}[\mathbf{x}_i - \mathbf{x}_b]. \quad (14)$$

The iterative process is terminated when $|(\chi_i^2 - \chi_{i-1}^2)/\chi_{i-1}^2| < 0.05$. A sounding is rejected if the solution has not converged within 8 iterations, when HIRS channels are included in the state vector, and within 3 iterations, when HIRS channels are not used.

(ii) *Residual check.* Here we check the difference between observed brightness temperatures and those computed with the current state estimate (referred to as a channel residual). For each channel, the ratio of the absolute value of the residual to the square root of its error variance is evaluated (referred to as the normalised residual). The normalized residuals are averaged over all included channels. If this quantity is greater than 1.0, indicating anomalously large residuals, the sounding is rejected.

(iii) *Saturation check.* At each iteration, we check for supersaturation within each layer. If a layer is supersaturated, we set its relative humidity equal to 100%. This restriction on the water vapour can inhibit convergence within the 1DVAR retrieval. In that case, the convergence check (i) will reject the sounding.

(iv) *Rain check.* After convergence, we attempt to eliminate soundings that indicate rain. This evaluation is based on the retrieved microwave surface emissivity. Because the microwave emissivity of land and sea ice is high relative to that over ocean and is similar to the values that would be retrieved in rain-contaminated scenes, we cannot perform this check over land or sea ice. Sea ice is eliminated from the open water cases by requiring the retrieved surface skin to be greater than 275 K. Rain is indicative of $\epsilon_{mw} > 0.7$. We therefore reject soundings matching these criteria. Very few soundings are rejected by this check, which is desirable, because it cannot be performed over land.

(v) *Surface temperature check.* Here we compare the retrieved (T_s^r) and background (T_s^f) surface skin temperatures. A sounding is rejected if $|T_s^r - T_s^f| > 3.5$ K over ocean or if $|T_s^r - T_s^f| > 15$ K over land or sea ice. Surface temperature differences larger than these values can indicate cloud contamination still present in the derived clear air radiances.

(vi) *η check.* In this test, we check the estimated values of η and corresponding noise amplification values A from (10) are not too large. If $\sqrt{A} > 10$, the sounding is rejected.

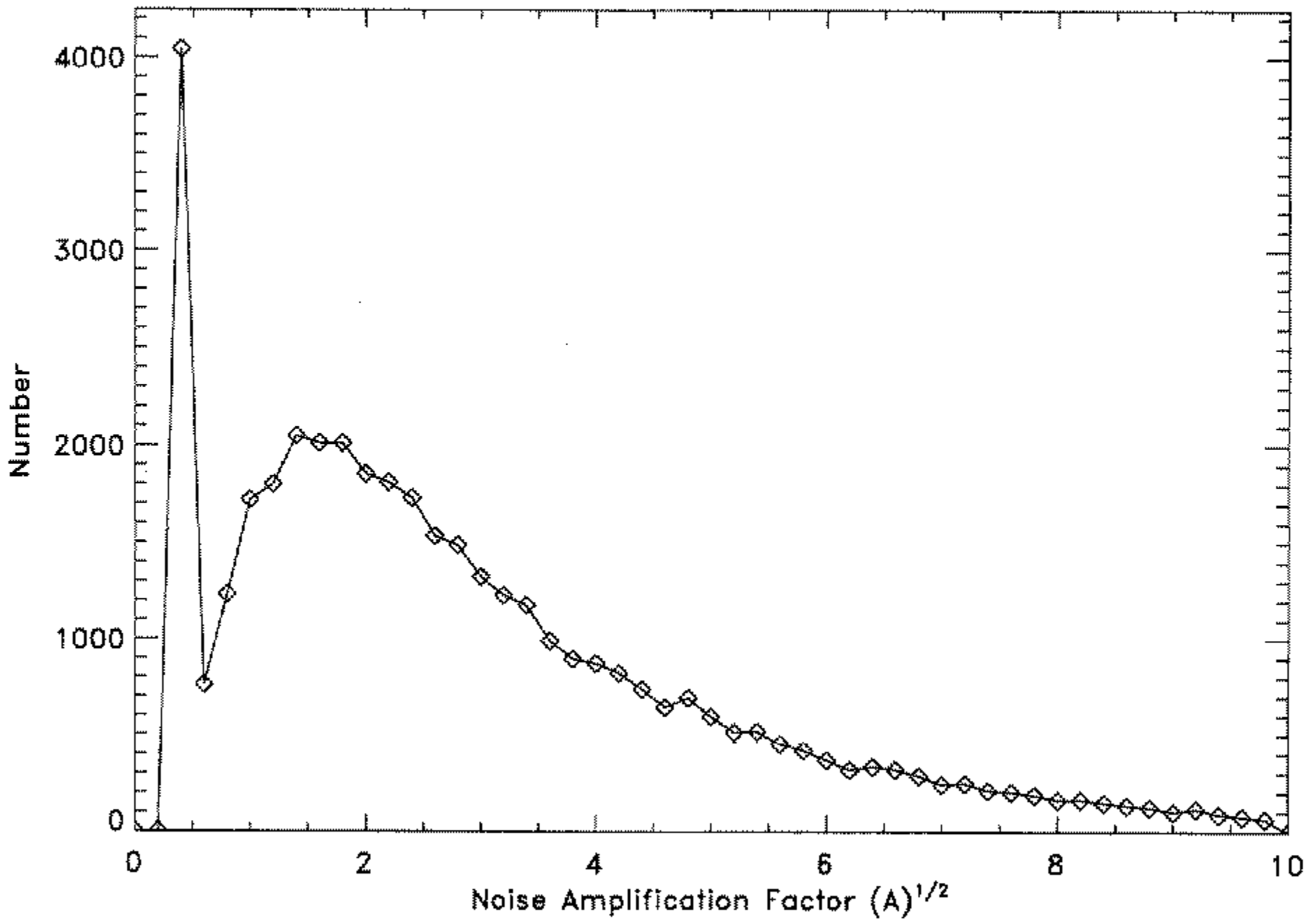

Figure 3. Histogram of noise amplification factor $A^{1/2}$ from NOAA-12 on 15 January 1992.

Figure 3 shows a histogram of $\sqrt{A}$. The peak near 0.6 is from clear soundings. The distribution peaks near $\sqrt{A} = 2$ and drops gradually to near zero by $\sqrt{A} = 10$.

(vii) *Gross check.* If the retrieved temperature at any level or the surface skin temperature exceeds 350 K or falls below 150 K, we reject the sounding. We also reject the sounding if the total ozone exceeds 650DU or falls below 90DU based on J. Gleason (private communication, 1997). These conditions are rarely met because the statistics constrain the solution, and the 1DVAR is more likely to fail one of the above checks.

(*d*) *Systematic error correction*

Systematic errors can be as large or larger than the random component of the instrument error. Systematic errors, or bias, can be accounted for within the 1DVAR framework (e.g. Dee and da Silva 1998). However, in our application, one generally attempts to remove bias prior to the analysis (e.g. Eyre 1992) or incorporates bias predictors into the analysis scheme (e.g. Derber and Wu 1998). We use the former strategy here. Collocated radiosonde data serve as our unbiased independent measurement. The details of our systematic error correction scheme are based on the work of Joiner (1997) and Joiner *et al.* (1998).

We use collocated radiosonde, satellite, and background (forecast) data for systematic error correction and routine monitoring of the 1DVAR. The radiosonde must have been launched within ± 3 hour and within 1° chordal distance of the satellite observation for successful collocation. Radiation corrections have not been applied to the radiosonde data. We discard certain manufacturer types of radiosondes from our sample (e.g. unknown) as a result of poor calibration and observed biases. The quality control marks applied to the temperature data by NCEP (Collins and Gandin 1996) are checked and used appropriately. Additional quality control checks were applied to screen out bad

radiosonde and TOVS observations. The above-mentioned cloud-detection checks were applied to TOVS observations and we used only those scenes determined to be clear for the bias correction.

Briefly, we compute coefficients for a small number of predictors (1–4) for each channel based on one month of collocated radiosonde data. These predictors correct for calibration and radiative transfer modeling errors. The predictors include scaling factors for water vapor and fixed gas optical depths, an offset to the satellite zenith angle, a constant, and secant of the satellite zenith angle. A subset of these predictors is chosen for each channel. In the present experiments, we used one month of radiosonde data to determine the bias coefficients.

One of the difficulties in using radiosonde data is that estimates of surface parameters, such as surface skin temperature and emissivity, are not provided. In our approach, we estimate these parameters simultaneously with the bias coefficients. With this approach, we must take care that we have enough information to estimate all of the parameters simultaneously. Therefore, we have to limit the number of bias predictors for surface-sensitive channels. For example, we do not have any bias predictors for MSU-1, because it is used to estimate the microwave emissivity affecting MSU-2. The different sensitivity of HIRS-8, 10, 18, and 19 to surface temperature, humidity, and fixed gases appears to enable the simultaneous determination of 1 or 2 bias predictors for these channels in addition to T_s and ρ (for daytime observations).

(e) *Contrast with previous approaches*

Channel selection has long been an important component of cloud-clearing approaches. Chahine (1977) illustrated that channels in the 15 μm CO_2 band should be used for cloud-clearing in combination with channels in the 4.3 μm CO_2 band for temperature sounding. Channels in the two CO_2 bands have different sensitivities to cloud and the resulting noise amplification effect as a result of the non-linear Planck function.

Our 1DVAR approach implicitly accounts for the sounding properties of channels in different bands through the observation operator, its Jacobian, and the observation error covariance. We have eliminated the need for channel selection, because all the channels are used simultaneously. The final solution for a successful sounding is therefore guaranteed to be consistent with all spectral measurements, and the approach is not dependent on any one set of channels.

4. Preliminary Non-Interactive Results

The results shown here are for NOAA 11 and NOAA 12 in January 1992. The 1DVAR results were obtained with a background from the forecasts of a previous GEOS-DAS experiment (i.e. the 1DVAR is non-interactive). In that experiment, NESDIS TOVS temperature retrievals were assimilated with other conventional data (i.e. our 1DVAR retrievals were not assimilated).

(a) *Cloud-cleared radiances and rejection statistics*

We first examine the cloudy and cloud-cleared brightness temperatures in HIRS 8, the 11 μm window channel, as an initial check. Figure 4 shows a cross-section through 2°S latitude of raw (FOV-3) and cloud-cleared HIRS 8 brightness temperatures on 15 January 1992 (a date chosen at random) from the NOAA-12 TOVS. FOV-3 is the cloudiest (clearest) FOV for scenes with clouds that are cooler (warmer) than the surface. The cooler brightness temperatures in the raw data indicate the presence of

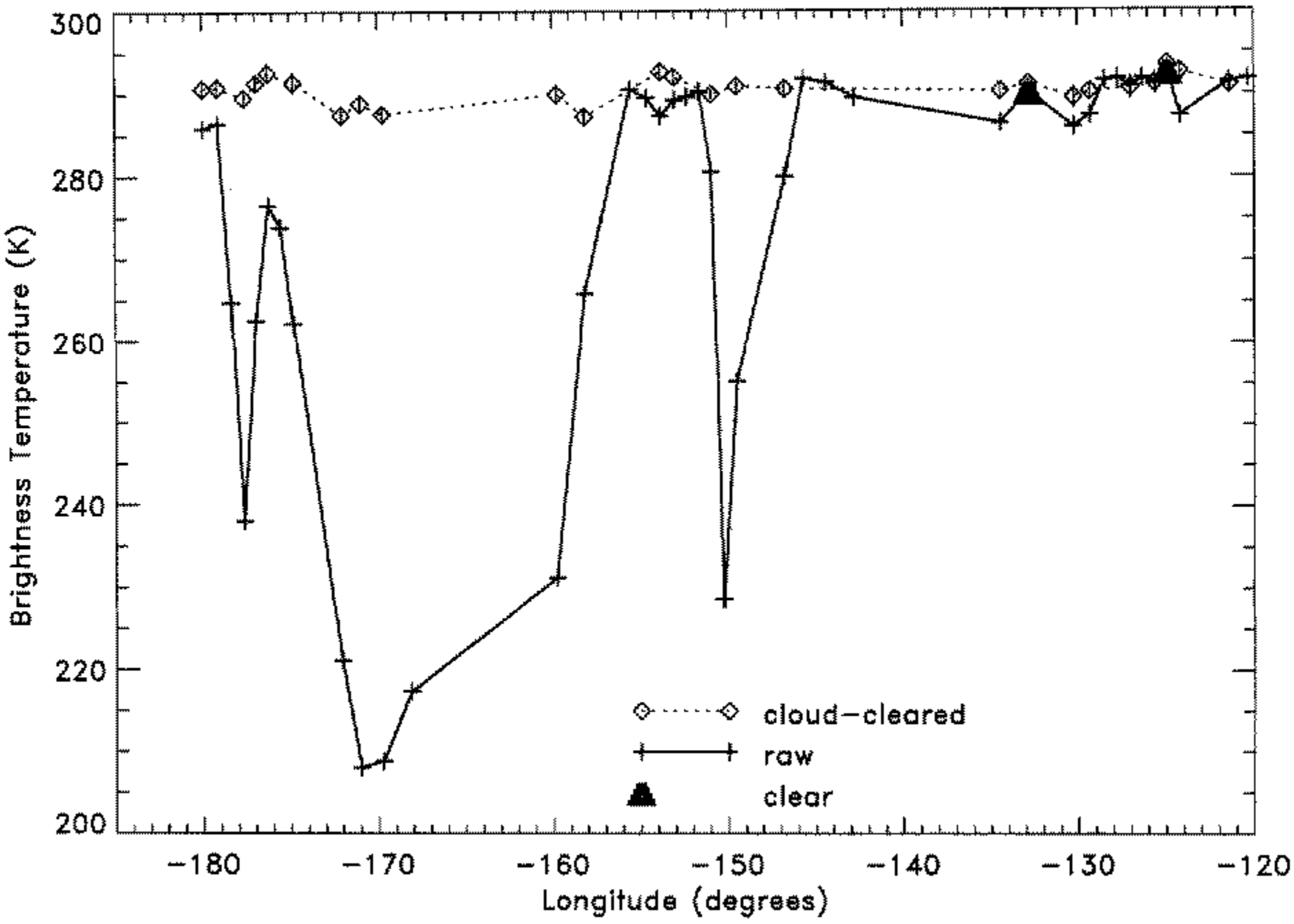

Figure 4. Cross-section of HIRS channel 8 raw, cloud-cleared (with error bars), and clear brightness temperatures, NOAA 12 satellite, 15 January, 1992 at 2°S latitude.

clouds that are emitting at colder temperatures than the surface. Gaps between three orbits can be seen.

The cloud-cleared brightness temperatures are mostly warmer and more homogeneous than the raw cloud-contaminated observations. Over ocean the cloud-cleared brightness temperatures are, as expected, close to the sea surface temperatures and close to those scenes declared cloud-free. This indicates that to first order, the 1DVAR is producing reasonable cloud-cleared brightness temperatures.

Cloud-cleared brightness temperatures are not shown for rejected soundings in Fig. 4. Some raw brightness temperatures that appear to be cloud-free have been rejected by the cloud-detection or cloud-clearing checks. In the future, we will revisit our checks to make sure that good data are not being rejected. For our 3×3 array of HIRS pixels, we classified approximately 6% of soundings as clear. All nine pixels, covering an area at nadir of approximately 2725 km^2, must indicate a clear scene to meet our cloud-free criteria. Our criteria for passing as clear is relatively tight, because we would rather classify a clear case as overcast than vice-versa. This is because the negative impact of a single erroneous observation in a data assimilation system can be more detrimental than the positive impact of one good observation. Conditions were flagged as overcast approximately 10% of the time. Slightly more than half of the cloud-cleared soundings pass all of the internal quality control checks. The majority of the rejected soundings failed the residual, surface temperature, or η checks. Overall, we accept approximately half the soundings with HIRS. This is significantly better coverage than is obtained using clear-only HIRS pixels at the individual pixel resolution.

(*b*) *Comparisons with radiosondes*

Satellite-derived 1D retrievals and their background fields have often been compared with collocated radiosonde data. However, such comparisons are often difficult

to interpret and may not be a good indicator of the usefulness of the data in assimilation systems. For example, TOVS is not expected to significantly improve upon the background estimate of the temperature profile in regions where *in situ* measurements are dense (e.g. Joiner and da Silva 1998). Therefore, we do not expect the collocated retrievals, especially those that have undergone cloud-clearing, to significantly improve upon the background with respect to radiosondes. In addition, if the 1DVAR retrievals are in error or if the radiance measurements or calculations or radiosonde data contain systematic errors, the 1DVAR retrievals can easily be slightly degraded with respect to the background (Eyre *et al.* 1993). Given these problems, we use radiosonde comparisons to check that the 1DVAR retrievals are not significantly degraded with respect to the background.

Figure 5 shows statistics for one month of collocated radiosonde temperature (layer mean) data. Data for clear and cloud-cleared soundings are shown separately. The standard deviation of the 1DVAR departures from the background are also shown. The departures, as expected, are relatively small and slightly larger in the lower troposphere for clear soundings. The larger increments in clear conditions are a result of the greater weight given to the radiances due to the lack of noise amplification. There is a slight bias in the GEOS background which is lessened at some altitudes by the 1DVAR. The standard deviation of the radiosonde minus 1DVAR is sightly reduced (at most altitudes) as compared with the background for both clear and cloud-cleared soundings.

We also obtained results in July 1988 with the NOAA-9 and -10 TOVS. There was no qualitative difference in the statistical results obtained with the NOAA-9 (even after MSU-2 failed), NOAA-10, NOAA-11, and NOAA-12 satellites. This shows that our approach is not dependent upon any one set of channels for cloud-clearing. Similar results are obtained with 1DVAR/radiosonde humidity comparisons.

(*c*) *Comparisons with ozone from UV measurements*

Comparison of TOVS-derived ozone with that from UV instruments provides a very useful validation of the cloud-clearing procedure. This is because the information about the ozone profile is derived mainly from HIRS-9. HIRS-9 is centred in the relatively weak 9.6 μm ozone band and is significantly affected by almost all of the parameters in the state vector (cloud-clearing parameters, the surface skin temperature and emissivity and atmospheric temperature, humidity, and ozone). Errors in any of these parameters as well as in cloud-detection and cloud-clearing will manifest themselves in the IR ozone retrieval.

With ultraviolet ozone-monitoring instruments, such as the Total Ozone Mapping Spectrometer (TOMS), surface and cloud effects can be modeled much more accurately than with IR measurements. TOMS, unlike HIRS 9, is relatively insensitive to the ozone profile shape at low and moderate solar zenith angles (e.g. Joiner *et al.* 1998). Therefore, TOMS produces high accuracy total column ozone (or total ozone) estimates. In contrast, TOVS requires prior information about the ozone profile in order to produce comparable total ozone estimates, because the HIRS-9 weighting function peaks in the lower stratosphere.

Here, the total column ozone (total ozone) derived from TOVS is compared with that from the Nimbus-7 TOMS instrument (McPeters *et al.* 1996). The results are separated into clear and cloud-cleared soundings. Some of the TOVS/TOMS differences result from temporal mismatches. The Nimbus-7 satellite was in a sun-synchronous orbit with a local crossing time near noon (TOMS makes measurements only in the presence of sunlight). The NOAA-11 and -12 satellites had specified local crossing times of 2:30 AM/PM and 7:30 AM/PM, respectively.

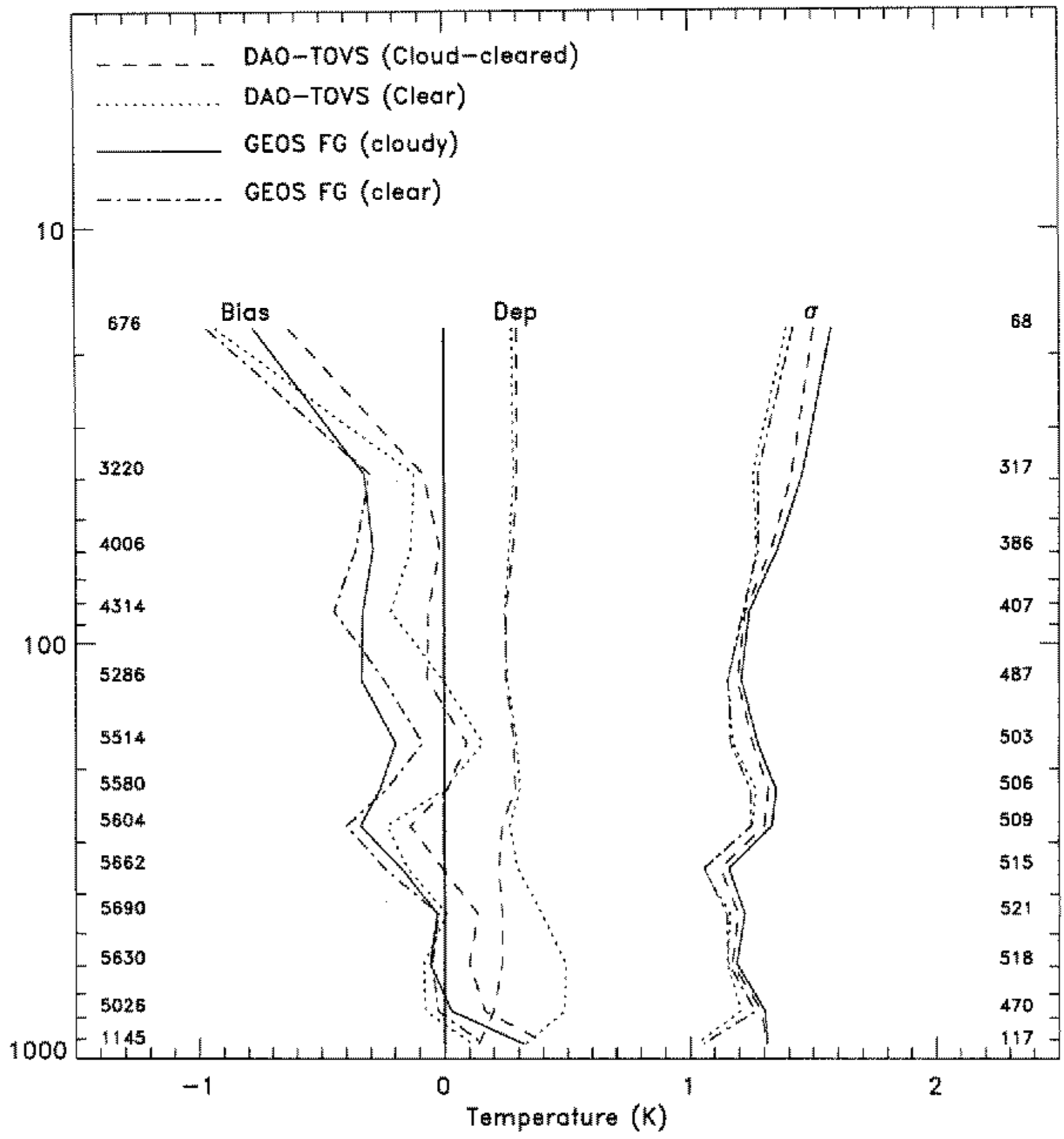

Figure 5. NOAA-12 Bias and standard deviation (σ) of radiosonde minus DAO-TOVS or GEOS background and standard deviation of the DAO-TOVS departure from the background (Dep) (layer mean values plotted at the layer midpoint between levels given in Table 2) averaged over December 1991; left: number of cloud-cleared collocated soundings; right: number of clear soundings.

Figures 6 and 7 show sample cross sections through 45°N latitude of the total ozone derived from the NOAA-11 and -12 TOVS, respectively, the Nimbus-7 TOMS, and that of the 1DVAR background on 15 January, 1992. At this latitude and time, variability in total ozone is large. An intrusion of low total ozone tropical air is present near 0° longitude. The overall agreement between TOMS and TOVS total ozone is reasonable, especially considering that the background is relatively crude and that no tuning of HIRS-9 with respect to the TOMS data has been applied. The only correction to the HIRS-9 radiance is a 30% change in the H_2O transmittance that was derived by Joiner *et al.* (1998).

The peak in total ozone near 50°E is shifted slightly to the south in the TOVS data. The shifts are different for the two satellites, indicating that this difference is due to temporal mismatch. Other peak shifts and differences can be seen between the two satellites. There does not appear to be much difference between the clear and cloud-cleared soundings in regions where both are present. There are a few places where both TOVS instruments measure significantly high or low as compared with TOMS. It is not clear whether this is due to errors in the first guess profile shape and statistics and/or

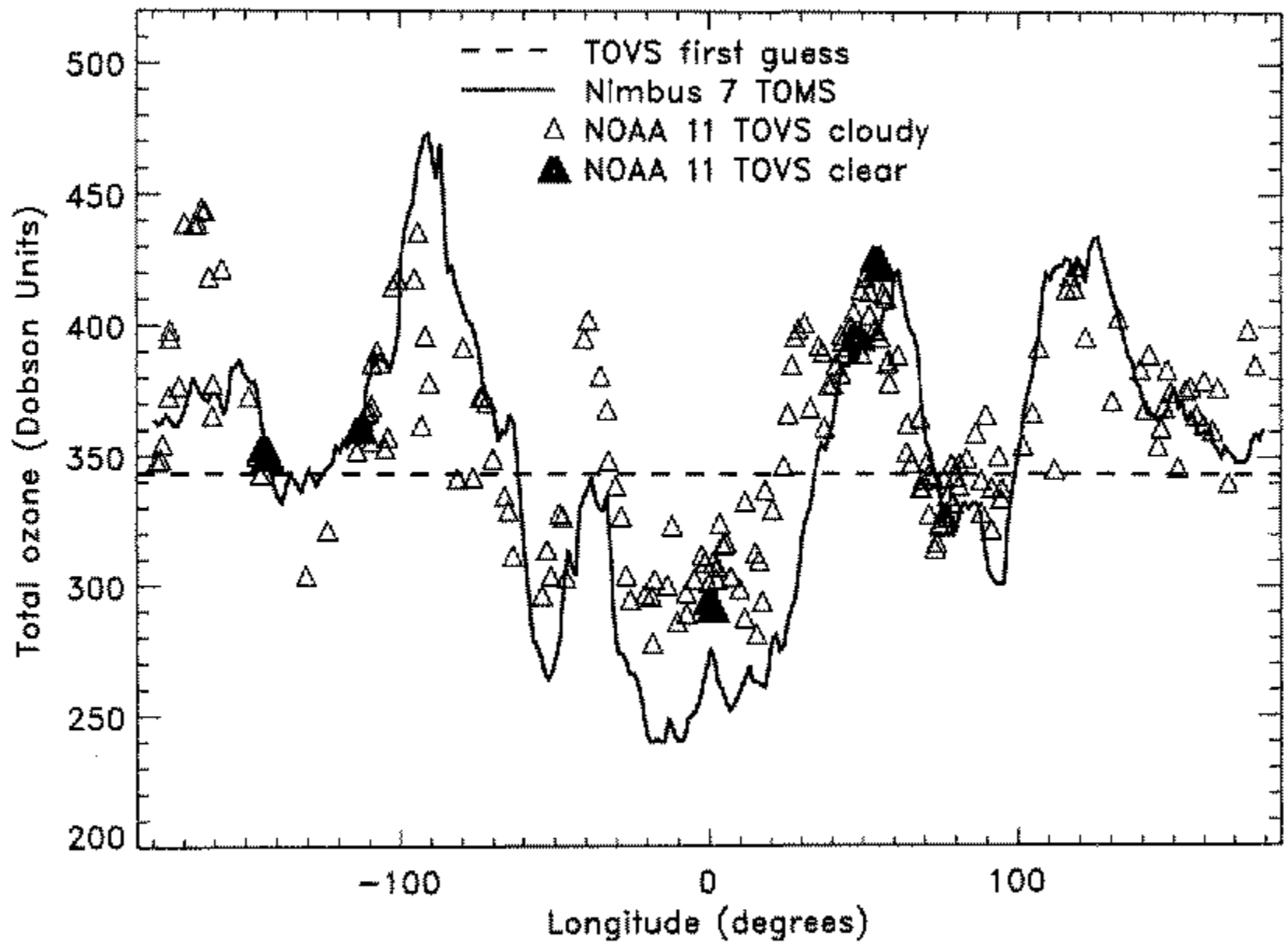

Figure 6. Total column ozone amounts from TOVS (NOAA-11 satellite) and TOMS and the climatological background in the TOVS 1DVAR at 45°N latitude on 15 January 1992 for clear and cloud-cleared soundings.

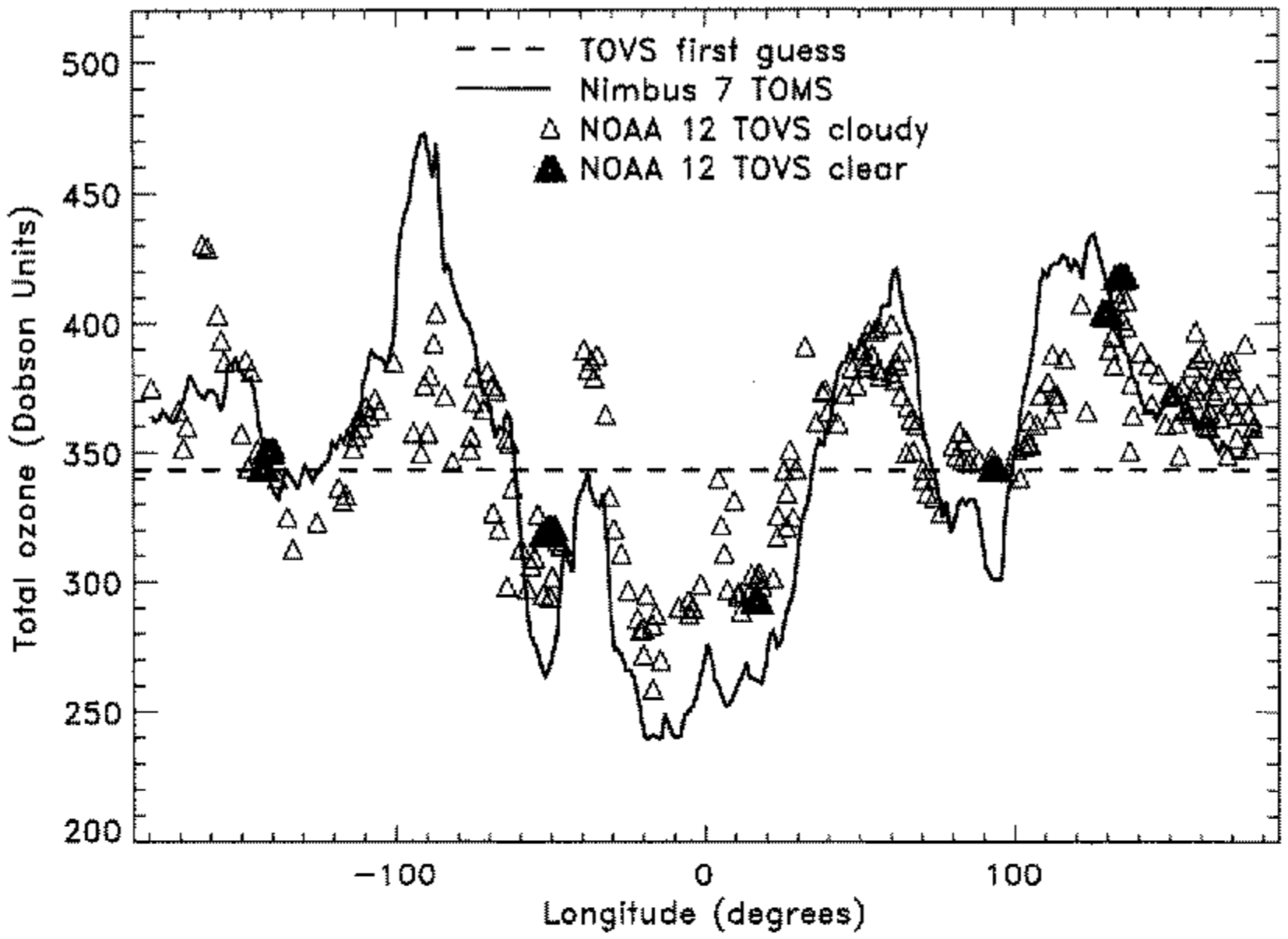

Figure 7. Same as in Fig. 6 but for NOAA-12.

some other problem. Profile shape errors can produce total ozone differences of this magnitude (Joiner *et al.* 1998).

Global statistics for six hour differences between the total ozone from the 1DVAR or climatological first guess and TOMS are listed in Table 3. The results are separated into clear and cloud-cleared soundings. In more than half the cases, the cloud-cleared statistics are actually better (mean, standard deviation, or both) than the clear statistics.

TABLE 3. BIAS AND STANDARD DEVIATION σ OF TOTAL COLUMN OZONE DIFFERENCES BETWEEN CLIMATOLOGICAL BACKGROUND (CLIM) OR 1DVAR (CLEAR = CLR, CLOUD-CLEARED = CC) AND TOMS

Satellite	Time period	clr bias (%)	clr σ (%)	cc bias (%)	cc σ (%)	all bias (%)	all σ (%)	clim bias (%)	clim σ (%)
NOAA 12	0Z	1.1	7.2	−0.3	7.9	−0.2	7.9	−1.6	12.7
NOAA 12	6Z	−5.1	11.2	−2.3	8.7	−2.6	9.0	−2.4	13.3
NOAA 12	12Z	−1.4	9.7	−1.0	8.1	−1.1	8.3	−1.5	11.5
NOAA 12	18Z	−0.8	7.1	−1.6	7.9	−1.5	7.9	−3.5	13.3
NOAA 11	0Z	−4.1	9.3	−1.8	8.6	−1.9	8.7	−1.6	11.4
NOAA 11	6Z	−4.3	9.9	−1.8	9.0	−1.9	9.0	−2.9	13.5
NOAA 11	12Z	−2.8	9.5	−1.8	8.8	−1.8	8.8	−2.3	12.6
NOAA 11	18Z	−3.3	8.5	−0.2	8.5	−0.3	8.5	−1.4	13.6

Both clear and cloud-cleared soundings significantly improve upon the first guess, indicating that there is useful information about O_3 in the cloud-cleared data. The average standard deviation of TOVS-TOMS total O_3 difference for a given day is typically about 8%. The TOVS-TOMS total O_3 bias in most cases is less than 2%. This bias is well within the absolute uncertainties of the TOMS- and TOVS-derived total ozone.

Chesters and Neuendorffer (1991) and Engelen and Stephens (1997) have made similar comparisons between TOMS and total ozone derived from TOVS. The TOVS/TOMS differences shown here are significantly less than those shown in the previous studies, both on a daily and monthly-mean basis. In addition, the TOVS/TOMS bias and standard deviation are close to the values predicted by Joiner *et al.* (1998). Based on their results, we expect a further reduction in the TOVS/TOMS difference using an improved prior estimate of the ozone profile.

(*d*) *Departure statistics*

Comparison of the differences between the 1DVAR and background (departures) for clear and cloud-cleared soundings away from radiosondes gives an indication of the usefulness of the cloud-cleared data. It also provides a check that clear and cloud-cleared departures are quantitatively similar, though we may expect slightly larger departures for clear soundings based on the larger weight given to the radiances.

Figure 8 shows histograms of 500 mb temperature departures at southern hemisphere latitudes greater than 60° separated into clear and cloudy cases. The statistics were generated from data on 15 January 1992. The cloud-cleared cases are further separated into two groups with noise amplification factors ($\sqrt{A}$) greater and less than three. The distributions are similar for all three cases with the clear scenes having slightly more populated wings and a slightly larger bias. All three have a negative bias and similar widths.

Figure 9 is similar to Fig. 8, but for 300 mb humidity at latitudes less than 30°. The distributions are more different in this case. This is due to the large noise amplification effect in HIRS-11 and -12 in cloudy cases. Even though the departures are smaller for cloudy cases, there still appears to be useful information in the cloudy data. All of the distributions show the GEOS forecast to be biased wet with respect to the 1DVAR results. This is consistent with a known wet bias in the GEOS model at these locations.

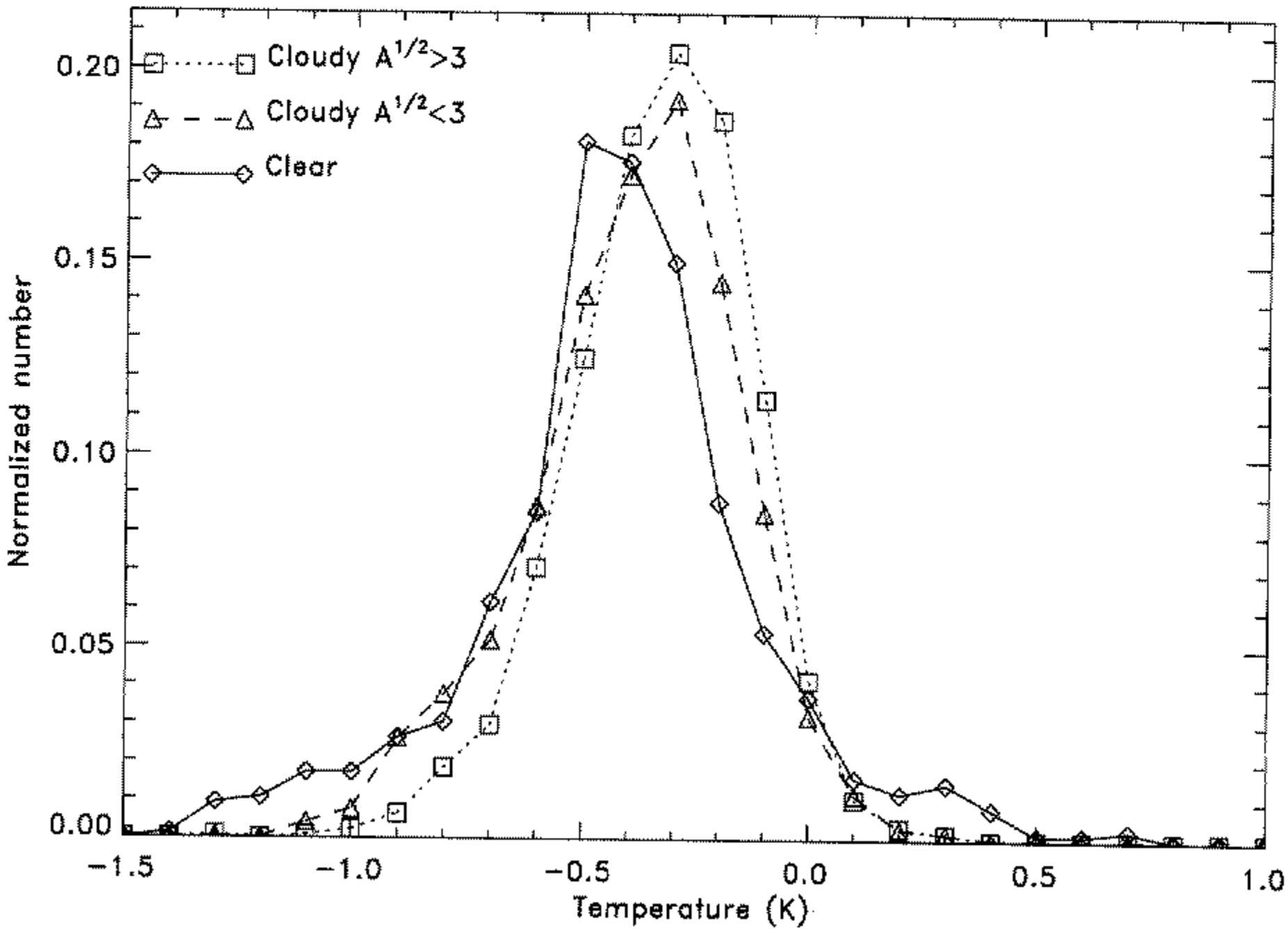

Figure 8. Histogram of NOAA-12 1DVAR minus GEOS first guess temperatures at 500 mb at latitudes south of 60°S on 15 January 1992. The y-axis is normalized by the total number of points.

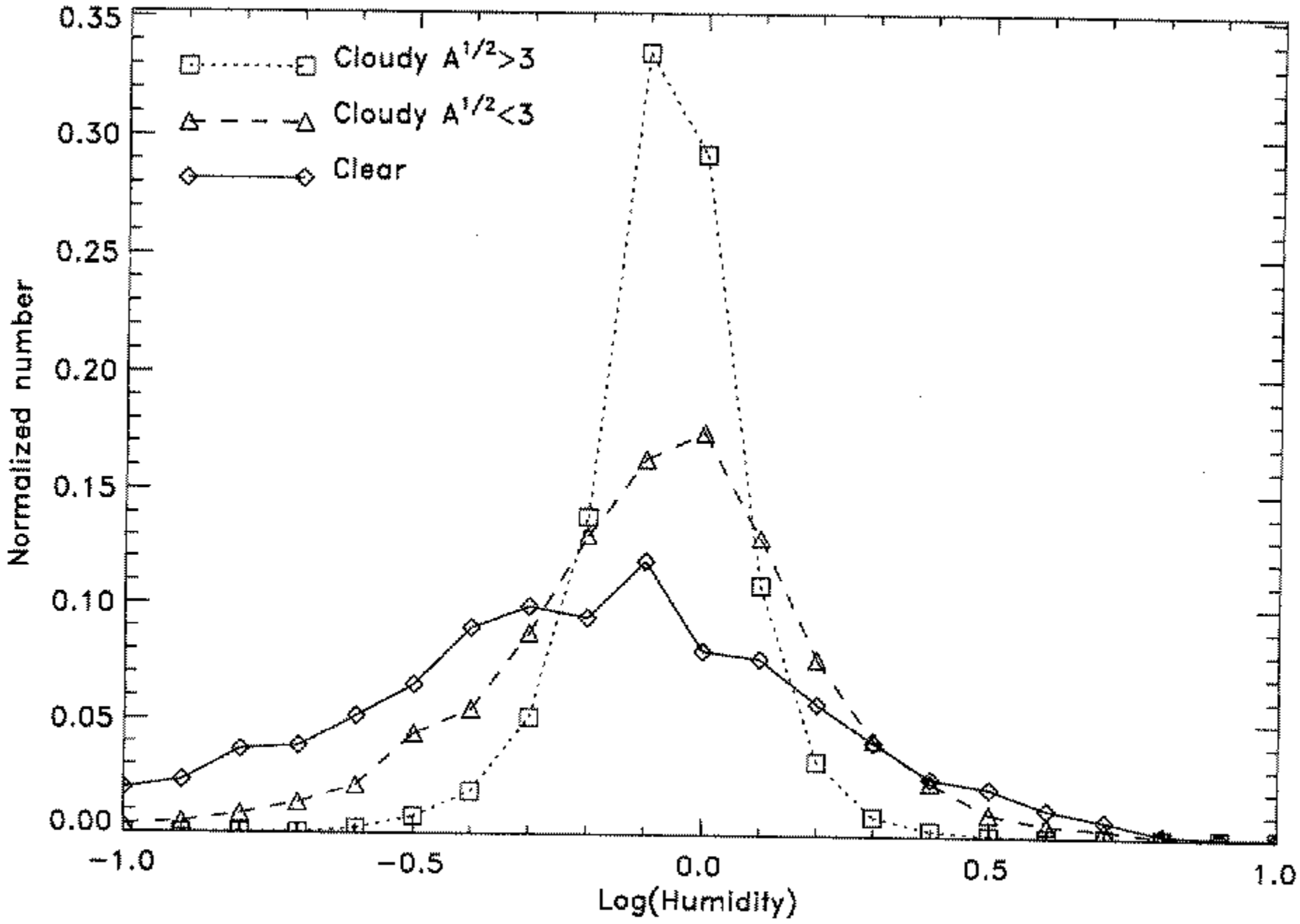

Figure 9. Similar to Fig. 8 except showing humidity departures (g/g) at 300 mb at latitudes less than 30°.

5. Conclusions and Future Work

We have used a variational framework to simultaneously cloud-clear infrared observations and retrieve information about the atmospheric and surface state. The approach is applied to TOVS data in 1-D. It can also be extended to 3- and 4-D analyses. Initial comparison of TOVS- and TOMS-derived total ozone provides evidence that the cloud-clearing scheme is performing well. Departure statistics indicate that there is useful information in the cloud-cleared data.

Experiments are currently being conducted in which the 1DVAR temperature and humidity information is assimilated into the GEOS-DAS. We will perform a series of tests, including forecast impact studies, to validate the 1DVAR results. The ultimate success of this approach can only be fully evaluated within a such DAS environment. The usefulness of cloud-cleared data can be assessed in experiments where the cloud-cleared data are and are not withheld from the DAS.

Acknowledgements

The authors would like to thank D. P. Dee, J. Susskind, J. Blaisdell, C. Barnet, R. B. Rood, M. Chen, A. da Silva, and G. Kelly for discussions, suggestions, and encouragement. The authors would also like to thank two anonymous revicwers and R. Saunders for helpful comments that improved the presentation of results.

References

Andersson, E. and Järvinen, H. 1998 Variational quality control. *Tech. Memo., 250*, ECMWF

Andersson, E., Pailleux, J., Thépaut, J. N., Eyre, J. R., McNally, A. P., Kelly, G. A. and Courtier, P. 1994 Use of cloud-cleared radiances in three/four-dimensional variational data assimilation. *Q. J. R. Meteorol. Soc.*, **120,** 627–653

Andersson, E., Haseler, J., Undén, P., Courtier, P., Kelly, G. A., Vasiljević, D., Branković, C., Cardinali, C., Gaffard, C., Hollingsworth, A., Jakob, C., Janssen, P., Klinker, E., Lanzinger, A., Miller, M., Rabier, F., Simmons, A., Strauss, B., Thépaut, J.-N. and Viterbo, P. 1998 The ECMWF implementation of three dimensional variational assimilation (3D-Var). III: Experimental results. *Q. J. R. Meteorol. Soc.*, **124,** 1831–1860

Chahine, M. T. 1974 Remote sounding cloudy atmospheres. I. The single cloud layer. *J. Atmos. Sci.*, **31,** 233–243

1977 Remote sounding cloudy atmospheres. II. Multiple cloud formations. *J. Atmos. Sci.*, **34,** 744–757

Chahine, M. T., Aumann, H. H. and Taylor, F. W. 1977 Remote sounding cloudy atmospheres. III. Experimental verifications. *J. Atmos. Sci.*, **34,** 758–765

Chesters, D. and Neuendorffer, A. 1991 Comparison between TOMS, TOVS and Dobson observations: satellite and surface views of total column ozone. *Palaeogeog., Palaeoclim., Palaeoecol.*, **90,** 61–67

Chu, W. P., McCormick, M. P., Lenoble, J., Brogniez, C. and Pruvost, P. 1989 SAGE II inversion algorithm. *J. Geophys. Res.*, **94,** 8339–8351

Collins, W. G. and Gandin, L. S. 1996 Complex quality control for observation errors of rawinsonde temperature and heights. Office Note 413. US Department of Commerce, NOAA-NWS, Environmental Modeling Center

Dee, D. P. and da Silva, A. M. 1998 Data assimilation in the presence of forecast bias, estimation of forecast and observation error covariance parameters. *Q. J. R. Meteorol. Soc.*, **124,** 269–295

Derber, J. C. and Wu, W.-S. 1998 The use of cloud-cleared radiances in the NCEP SSI analysis system. *Mon. Weather Rev.*, **126,** 2287–2299

Engelen, R. J. and Stephens, G. L. 1997 Infrared radiative transfer in the 9.6 μm band: Application to TIROS operational vertical sounder ozone retrieval. *J. Geophys. Res.*, **102,** 6929–6939

Eyre, J. R. 1989a Inversion of cloudy satellite sounding radiances by nonlinear optimal estimation. I. Theory and simulation for TOVS. *Q. J. R. Meteorol. Soc.*, **115,** 1001–1026

1989b Inversion of cloudy satellite sounding radiances by nonlinear optimal estimation. II. Application to TOVS data. *Q. J. R. Meteorol. Soc.*, **115,** 1027–1037

1991 A fast radiative transfer model for satellite sounding systems. *ECMWF Tech. Memo. 176*, ECMWF, Reading, UK

1992 A bias correction scheme for simulated TOVS brightness temperatures. *ECMWF Tech. Memo 186*, ECMWF, Reading, UK

Eyre, J. R. and Watts, P. D. 1987 A sequential estimation approach to cloud-clearing for satellite temperature sounding. *Q. J. R. Meteorol. Soc.*, **113,** 1349–1376

Eyre, J. R., Kelly, G. A., McNally, A. P., Andersson, E., and Persson, A. 1993 Assimilation of TOVS radiance information through one-dimensional variational analysis. *Q. J. R. Meteorol. Soc.*, **119,** 1427–1463

Jazwinski, A. H. 1970 *Stochastic processes and filtering theory*. Academic Press, New York, USA

Joiner, J. 1997 Investigation of systematic errors and correction models. Pp. 207–216 in *Proc. 9th Internat. TOVS Study Conf.*, Igls, Austria. Eds. J. R. Eyre and M. Uddstrom

Joiner, J., Lee, H.-T., Strow, L. L., Bhartia, P. K., Hannon, S., Miller, A. J. and Rokke, L. 1998 Radiative transfer in the 9.6 micron HIRS ozone channel using collocated SBUV-determined ozone abundances. *J. Geophys. Res.*, **103,** 19213–19229

Joiner, J. and da Silva, A. M. 1998 Efficient methods to assimilate remotely-sensed data based on information content. *Q. J. R. Meteorol. Soc.*, **125,** 1669–1694

Kidwell, K. B., Ed. 1997 NOAA Polar Orbiters Data User's Guide, August 1997 Revision. US Department of Commerce, NOAA-NESDIS, *NCDC/CSD/SSB* Suitland, MD.

Lorenc, A. C. 1986 Analysis methods for numerical weather prediction. *Q. J. R. Meteorol. Soc.*, **112,** 1177–1194

McMillin, L. M. and Fleming, H. E. 1976 Atmospheric transmittance of an absorbing gas: Part 1. A computationally fast and accurate transmittance model for absorbing gases with constant mixing ratios in inhomogeneous atmospheres. *Appl. Opt.*, **15,** 358–363

McMillin, L. M. and Dean, C. 1982 Evaluation of a new operational technique for producing clear radiances. *J. Appl. Meteorol.*, **21,** 1005–1014

McNally, A. P., Derber, J. C., Wu, W. and Katz, B. B. 2000 The use of TOVS level-1b radiances in the NCEP SSI analysis system. *Q. J. R. Meteorol. Soc.*, **126,** 689–724

McPeters, R. D., Krueger, A. J., Bhartia, P. K., Herman, J. R., Oaks, A., Ahmad, Z., Cebula, R. P., Schlesinger, B. M., Swissler, T., Taylor, S., Torres, O. and Wellemeyer, C. G. 1996 Nimbus-7 total ozone mapping spectrometer (TOMS) data products user's guide. *NASA Ref. Publ., 1384*

Reynolds, R. W. 1988 A real time global sea surface temperature analysis. *J. Clim.*, **1,** 75–86

Rodgers, C. D. 1976 Retrieval of atmospheric temperature and composition from remote measurements of thermal radiation. *Rev. Geophys. and Space Phys.*, **14,** 609–624

Saunders, R., Matricardi, M. and Brunel, P. 1999 An improved fast radiative transfer model for assimilation of satellite radiance observations. *Q. J. R. Meteorol. Soc.*, **125,** 1407–1425

Sienkiewicz, M. 1996 The GLA TOVS Rapid Algorithm Forward Radiance Modules and Jacobian Version 1.0, *DAO Office Note 96-08*, Data Assimilation Office, Goddard Space Flight Center, Greenbelt, MD, USA

Smith, W. L. 1968 An improved method for calculating tropospheric temperature and moisture from satellite radiometer measurements. *Mon. Weather Rev.*, **96,** 387–396

Smith, W. L., Knuteson, R. O., Revercomb, H. E., Feltz, W., Howell, H. B., Menzel, W. P., Nalli, N. R., Brown, O., Brown, J., Kinnett, P. and McKeown, W. 1996 Observations of the infrared radiative properties of the ocean-implications for the measurements of sea surface temperature via satellite remote sensing. *Bull. Am. Meteorol. Soc.*, **77,** 41–51

Smith, W. L., Woolf, H. M., Hayden, C. M., Wark, D. Q. and McMillin, L. M. 1979 The TIROS-N operational vertical sounder. *Bull. Am. Meteorol. Soc.*, **60,** 1177–1187

Susskind, J., Rosenfield, J. and Reuter, D. 1983 An accurate radiative transfer model for use in the direct physical inversion of HIRS and MSU temperature sounding data. *J. Geophys. Res.*, **88,** 8550–8568

Susskind, J., Rosenfield, J., Reuter, D. and Chahine, M. T. 1984 Remote sensing of weather and climate parameters from HIRS2/MSU on TIROS-N. *J. Geophys. Res.*, **89,** 4677–4697

Susskind, J. and Reuter, D. 1985 Intercomparison of physical and statistical retrievals from simulated HIRS2 and AMTS data. P. 641 in A. Deepak, H. E. Fleming and M. T. Chahine (eds.). Advances in remote sensing retrieval methods. A. Deepak, Hampton VA

Takacs, L. L., Molod, A. and Wang, T. 1994 Documentation of the Goddard Earth Observing System (GEOS) general circulation model—version 1. *NASA Tech. Memo. 104606, Vol. 1*, Ed. M. J. Suarez. Linthicum Heights, MD, USA

Talagrand, O. 1988 Four-dimentional variational assimilation. Pp. 1–30 in Proc. ECMWF Seminar on data assimilation and the use of satellite data, Vol. 2. Reading

Wylie, D. P., Menzel, W. P., Woolf, H. M. and Strabala, K. I. 1994 Four years of global cirrus cloud statistics using HIRS. *J. Clim.*, **7,** 1972–1986

Wu, Z. J. and McAvaney, B. 1998 Simulation of impacts of climatological MSU data processing methods using NCEP/NCAR reanalysis data. *J. Geophys. Res.*, **103,** 19495–19508